The Astrophysical Journal, 739:92 (7pp), 2011 October 1 doi:10.1088/0004-637X/739/2/92

KINK WAVES IN AN ACTIVE REGION DYNAMIC FIBRIL

A. Pietarila[1], R. Aznar Cuadrado[2], J. Hirzberger[2], and S. K. Solanki[2,3]
[1] National Solar Observatory, 950 N. Cherry Avenue, Tucson, AZ 85719, USA
[2] Max-Planck-Institute for Solar System Research, Max-Planck-Strasse 2, 37191 Katlenburg-Lindau, Germany
Received 2011 April 26; accepted 2011 July 12; published 2011 September 14

ABSTRACT

We present high spatial and temporal resolution Ca II 8542 Å observations of a kink wave in an on-disk chromospheric active region fibril. The properties of the wave are similar to those observed in off-limb spicules. From the observed phase and period of the wave we determine a lower limit for the field strength in the chromospheric active region fibril located at the edge of a sunspot to be a few hundred gauss. We find indications that the event was triggered by a small-scale reconnection event higher up in the atmosphere.

Key words: Sun: chromosphere – Sun: oscillations – sunspots

Online-only material: color figure

1. INTRODUCTION

Recent observations have strengthened the connection between spicules and coronal heating, either via spicules supplying hot plasma to the corona (De Pontieu et al. 2011) or energy dissipation from MHD waves propagating along spicules (e.g., Kukhianidze et al. 2006; De Pontieu et al. 2007; He et al. 2009). The first observations of transverse oscillations, indicative of MHD waves, in spicules were made already in the late 1960s (Pasachoff et al. 1968). Since the discovery that MHD waves are fairly ubiquitous in spicules (De Pontieu et al. 2007) the interest has been renewed. For a recent observational review of spicule oscillations see Zaqarashvili & Erdélyi (2009). Several authors, e.g., De Pontieu et al. (2007) and He et al. (2009), have identified the waves as kink or Alfvén and estimated that they carry enough energy to heat the corona.

Based on theoretical considerations we expect to find four different modes of waves in cylindrical plasma geometries appropriate for solar conditions: kink, sausage, longitudinal, and torsional. The first three modes are compressible, while the fourth one is not. All of the modes have been observed in the solar corona (although the identification of the pure, and thus incompressible, Alfvén waves has been questioned by Van Doorsselaere et al. 2008). Alfvén and kink waves can be triggered by granular buffeting of photospheric magnetic flux tubes (e.g., Roberts 1979; Hollweg 1981; Spruit 1981; Choudhuri et al. 1993; Huang et al. 1995; Musielak & Ulmschneider 2001) or by small-scale reconnection (Axford & McKenzie 1992). Differentiating observationally between kink and Alfvén wave modes is not entirely straightforward since both can cause transversal displacements and observationally appear as incompressible, at least for some magnetic field geometries (Van Doorsselaere et al. 2008). In general, these wave modes can be distinguished in straight, cylindrical, high density magnetic flux tubes. Flux tubes act as wave guides for kink waves (i.e., the wave is confined in the tube), which in turn cause transverse displacements of the tube axis. In contrast, Alfvén waves propagating incompressibly along a magnetic flux tube are torsional and do not lead to a transversal displacement (Erdélyi & Fedun 2007; Van Doorsselaere et al. 2008). Chromospheric kink and Alfvén waves have been observed in off-limb spicules. Since fibrils are the likely on-disk counterpart of spicules (e.g., Tsiropoula et al. 1994) one would expect to see transverse oscillations in them as well.

The observed properties of MHD waves can be used to measure the magnetic field strength in, e.g., coronal loops (e.g., Nakariakov & Ofman 2001) as well as spicules (e.g., Zaqarashvili et al. 2007; Singh & Dwivedi 2007; Kim et al. 2008). The thus measured spicule field strengths outside active regions are generally in the 10–40 G range. Spectropolarimetric measurements of spicules yield similar field strengths, e.g., 10 G from Hanle measurements of the He I 10830 Å triplet (Trujillo Bueno et al. 2005) and 30 G from He I D3 measurements (López Ariste & Casini 2005). In this paper, we present observations of transverse oscillations in on-disk fibrils, and based on them give an estimate of the magnetic field strength in chromospheric active region dynamic fibrils.

2. OBSERVATIONS AND DATA ANALYSIS

The main goal of the observing sequence was to study the chromosphere on small spatial and temporal scales using the Ca II 8542 Å line. The line wings sample the photosphere up to the reversed granulation, while the line core is formed in the chromosphere. Because of its sensitivity to velocities, temperatures, and magnetic fields, the Ca II 8542 Å line is a powerful tool for chromospheric studies.

We observed active region AR 11019 ($x = -342''$ and $y = 397''$, $\mu = 0.87$) with the CRisp Imaging SpectroPolarimeter (CRISP; Scharmer 2006) at the Swedish Solar Telescope on 2009 June 2 from 08:15 UT to 08:50 UT. The observing sequence, optimized for fast chromospheric dynamics, consisted of a main sequence of rapid Dopplergrams (at ±180 mÅ from line core) of the Ca II 8542 Å line with a more thorough spectral scan (referred to as the background, BG, scan) interwoven into it. Details are given in Table 1. In practice, we alternated between the two scans, i.e., every second wavelength of the series was either the red or blue point of the Dopplergram scan and the remaining points made up the background scan. Every 5.3 minutes the Fe I 6302 Å line was scanned to provide a photospheric context. The transmission profile of the instrument is 107.3 mÅ at 8540 Å and 53.5 mÅ at 6300 Å. The pixel size is 0.″0592. For each image recorded by CRISP a wide-band (2 Å) intensity image was simultaneously recorded with a separate camera. These were later used to co-align the data set and to

[3] Also at School of Space Research, Kyung Hee University, Yongin, Gyeonggi, 446-701, Korea.

Table 1
Observations

Scan	$\lambda - \lambda_0$ (mÅ)	Cadence (s)
Ca II 8542 Å, Dopp	±180	3.4
Ca II 8542 Å, BG	±750, ±450, ±350, ±250, ±180, ±90, 0, 2000	21
Fe I 6302 Å	±120, ±60, 0, 680	320

destretch it to remove artifacts caused by the varying seeing conditions following the method described by Yi et al. (1992).

Adaptive optics (AOs; Scharmer et al. 2003) were used during the observations and the recorded images were reconstructed using multi-object multi-frame blind deconvolution (MOMFBD; van Noort et al. 2005) resulting in images with very high spatial resolution (≈0.″21, which corresponds basically to the diffraction limit of the SST at 8540 Å). For most of the time the seeing conditions were good and stable, but they began to gradually deteriorate toward the end of the observations.

For the spectropolarimetric data instrumental polarization effects of the laboratory setup were measured with dedicated calibration optics. Additionally, for the Fe I 6302 Å data the telescope polarization was determined using a model developed by Selbing (2005). No telescope model is currently available for Ca II 8542 Å so this step was omitted in the Ca II 8542 Å reduction. These demodulation matrices were applied to the data resulting in the full Stokes vectors for the observed wavelength points for each pixel.[4]

3. RESULTS

The main feature in the observed field of view (roughly 40 Mm × 40 Mm) is AR 11019 (Figure 1). It consists of some pores and a sunspot with only very few penumbral fibrils. The region of interest (ROI; outlined in Figure 1) is on the edge of the main spot. There are no large concentrations of magnetic field of either polarity to the right of the observed region in the Michelson–Doppler Imager (MDI) magnetogram taken 10 minutes before the observations. The following spot is located on the opposite side of the observed main spot from the ROI.

A comparison of the Fe I 6302 Å and Ca II 8542 Å Stokes *V* images in Figure 1 reveals a few locations, e.g., around position (24,22) Mm and (21,16) Mm, where the two appear to have seemingly opposite polarities. These may be a result of emission in the Ca II 8542 Å line rather than a genuine change in polarity of the magnetic field as pointed out by Sánchez Almeida (1997).

3.1. Atmospheric Structure and Dynamics in the ROI

The main chromospheric features in the ROI (Figure 2) are fibrils originating from the spot and extending nearly radially away from it. Most of the magnetic field to the right of the spot in and around the ROI is unipolar. It is unlikely that many fibrils (assuming that they outline the magnetic field) in the ROI connect back to the photosphere inside or near the observed area.

Dynamic fibrils and rapid blueshifted events are seen in movies of the Ca II 8542 Å intensities. Dynamic, dark (when viewed in line wing intensities) fibrils are seen relatively often. Usually they are located some distance away from the spot and do not connect to it. An exception is seen in image sequences of the red wing of Ca II 8542 Å in Figure 2: a collection of very dark fibrils connect to the spot and are marked by the vertical arrows (to avoid confusion, hereafter this collection of fibrils will be referred to as FOI, fibrils of interest). Two to three individual fibrils make up the FOI which all together are around 1″ in width. The FOI are visible in movies of the wavelength points redward of the line core. When viewed in movies of intensity at +750 mÅ the FOI start as faint fibrils which

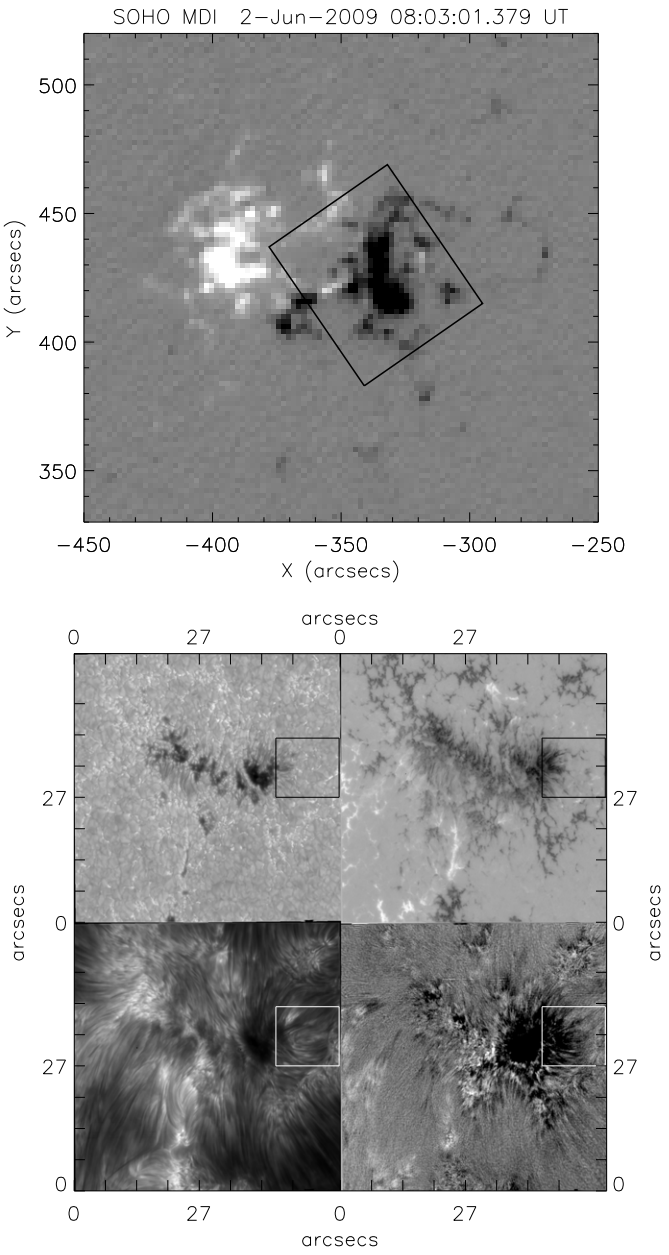

Figure 1. Top frame: MDI magnetogram (color scale is −700–700 G). The square marks the approximate location of the SST FOV. Bottom frame: field of view observed by CRISP (images taken at 08:25 UT). Top left subframe: wide-band (photospheric) intensity near Ca II 8542 Å. Top right subframe: Stokes *V* at −60 mÅ from the Fe I 6302 Å core. Bottom left subframe: intensity at −90 mÅ from the Ca II 8542 Å core. Bottom right subframe: Stokes *V* at −90 mÅ from the Ca II 8542 Å core. The squares in each panel mark the location of the region of interest (ROI). Note that the top frame is rotated ≈80° counterclockwise compared to the frames below.

[4] Comparison of the Fe I 6302 Å and Ca II 8542 Å Stokes *V* signals shows that the Ca II 8542 Å circular polarization data are not severely affected by instrumental polarization effects and can be used, at least, for purely qualitative purposes (Figure 1). Because of the much smaller signals, the Ca II 8542 Å linear polarization signal cannot be used without first applying a proper telescope model.

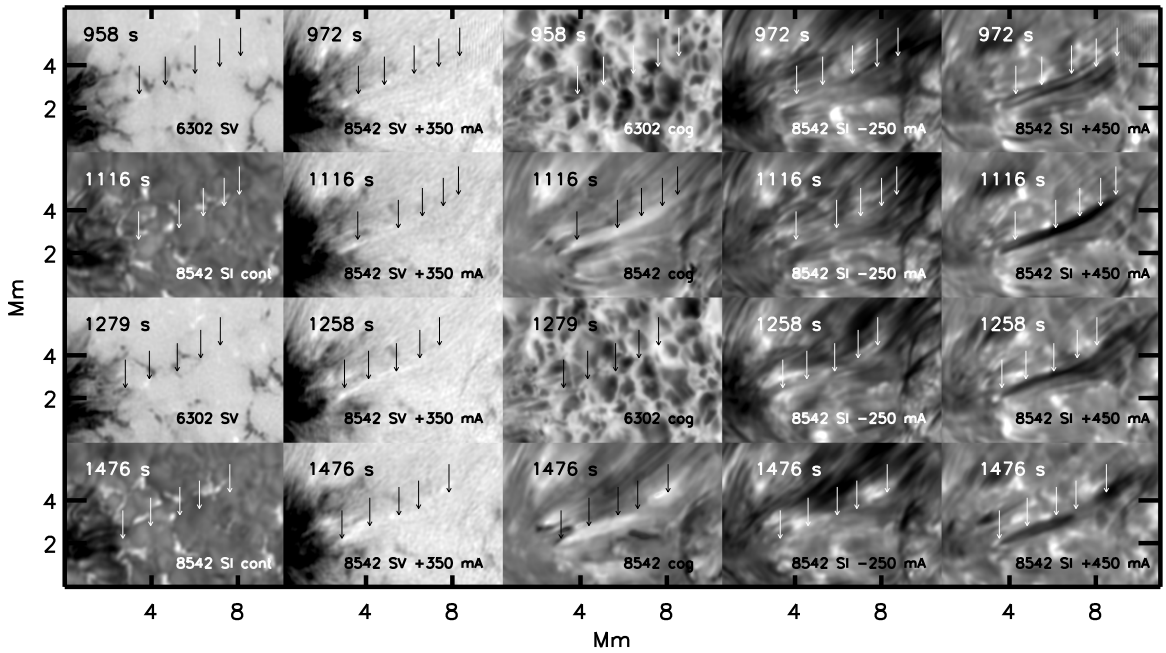

Figure 2. ROI. 1st column: alternating Fe I 6302 Å Stokes *V* signal and wide-band intensity near Ca II 8542 Å. 2nd column: Ca II 8542 Å Stokes *V* at +350 mÅ. 3rd column: alternating Fe I 6302 Å COG λ (scaled to ± 1.9 km s^{-1}) and Ca II 8542 Å COG λ (scaled to ± 7 km s^{-1}). 4th column: Ca II 8542 Å Stokes *I* at −250 mÅ. 5th column: Ca II 8542 Å Stokes *I* at +450 mÅ. Observing time (in seconds from $t = 0$) is given at the bottom of each image. The arrows point to the location of the FOI.

merge, become darker, and eventually retract into the spot. The footpoint (discussed in more detail in Section 3.4) of the FOI is brighter than the surroundings and after the FOI connect with the spot, the footpoint momentarily has positive polarity in Ca II 8542 Å magnetograms. This does not necessarily imply a fleeting change in the polarity of the magnetic field, but is more likely associated with an inversion in the line core due to transient heating of the chromosphere at this location (Sánchez Almeida 1997).

3.2. Periodic Transverse Displacement of FOI

Figure 3 shows *xt*(space-time)-cuts (artificial slit time series) of the Dopplergrams placed perpendicular to the FOI. The FOI start as a single dark feature moving toward the upper part of the ROI (right in the *xt*-cut) with an apparent transverse speed of approximately 2 km s^{-1}. The movement is at first best seen in the blue wing and later in the red as well. At $t = 300$ s the feature splits into multiple strands which oscillate transversely. The oscillations last ≈10 minutes after which the FOI disappear from the *xt*-cut, i.e., no damping in time of the oscillations is seen. In the ROI the FOI continue to retract and eventually (at the end of the observing sequence) disappear entirely into the footpoint. The coherent motions with a period of ≈20 s in the FOI are caused by seeing conditions.

Measurements of the fibrils' trajectories in the red wavelength point are made from *xt*-cuts placed perpendicular to the FOI or along the vertical direction (no interpolation of data was made) at various positions along the feature (positions of slits are shown in far left panel of Figure 3). The trajectories are identified by eye from each *xt*-cut. When a clear periodicity is visible in the trajectory, a single sine wave and a linear function that accounts for any lateral movement of the FOI are fitted to the trajectory. The fit returns a period, amplitude, and phase relative to $t = 0$. A transverse velocity (amplitude/period) for the swaying motion is also computed. The results of the fits are shown in Figure 4. The period varies between two to three minutes, with a mean value of 135 s. The mean apparent speed is 1 km s^{-1}. The phase and distance to the footpoint are not strongly correlated (Pearson correlation coefficient, r_c, is −0.26): the propagation is either too fast to be measured robustly on such small spatial scales or the perturbation does not propagate. The perpendicular to FOI phase measurements show, however, a more consistent decreasing trend in the interval (4.4–5.7 Mm). An ordinary linear least-squares bisector fit to the phase as a function of distance to the footpoint gives a slope of -5.26 ± 1.11 s Mm^{-1} giving a phase speed of −190 km s^{-1}. (Note that the inferred slope depends on which method is used to calculate the linear regression coefficients giving rise to a larger uncertainty than quoted above.) This together with the negative correlation coefficient indicate that if the perturbation propagates, the propagation is toward the footpoint.

We use the Dopplergrams to identify the locations in space and time and interpolate them to the background scan to identify the FOI pixels. Compared to the plage-dominated surroundings, the Stokes *I* profiles in the FOI are deeper, redshifted, and more asymmetric, i.e., the red wing is broader than the blue wing (Figure 5). The difference between the FOI and surrounding intensity profiles is largest at +250 mÅ. This is also seen in measurements of the FWHM and center of gravity wavelength (COG λ). The median FWHM and COG λ in the FOI are 770 mÅ and 32 mÅ (corresponds to 1.4 km s^{-1}), respectively, compared to 615 mÅ and −17 mÅ (−0.6 km s^{-1}) in the surrounding ROI (excluding the spot). (Note that zero wavelength and velocity are not calibrated, so the COG λ values are only relative.) The FOI pixels closest to the footpoint tend to have largest FWHM and COG λ; perhaps the material is accelerated as it retracts to the footpoint or the FOI is more vertical near the footpoint.

3.3. Magnetic Field Strength in FOI

The expression for kink waves in a vertical thin flux tube (Nakariakov & Verwichte 2005) gives a relation between the

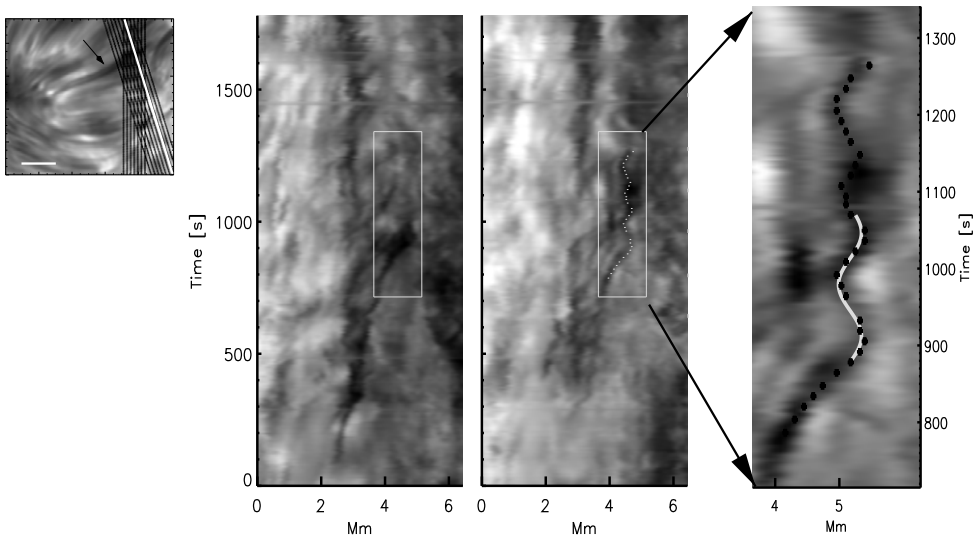

Figure 3. Transverse oscillations of the FOI. Locations of the xt-cuts in the ROI (at +180 mÅ from line core) are on the left (white marks location of cuts shown in this figure, black shows location of all xt-cuts). The separate horizontal white line marks the scale of 2 Mm. The black arrow points to the FOI. Middle two panels: xt-cuts (at −180 mÅ left and at +180 mÅ right, from Ca II 8542 Å core). Right panel: magnification of area in the white rectangle. The black crosses are the measured trajectory and the white line shows the sine wave fitted to the trajectory.

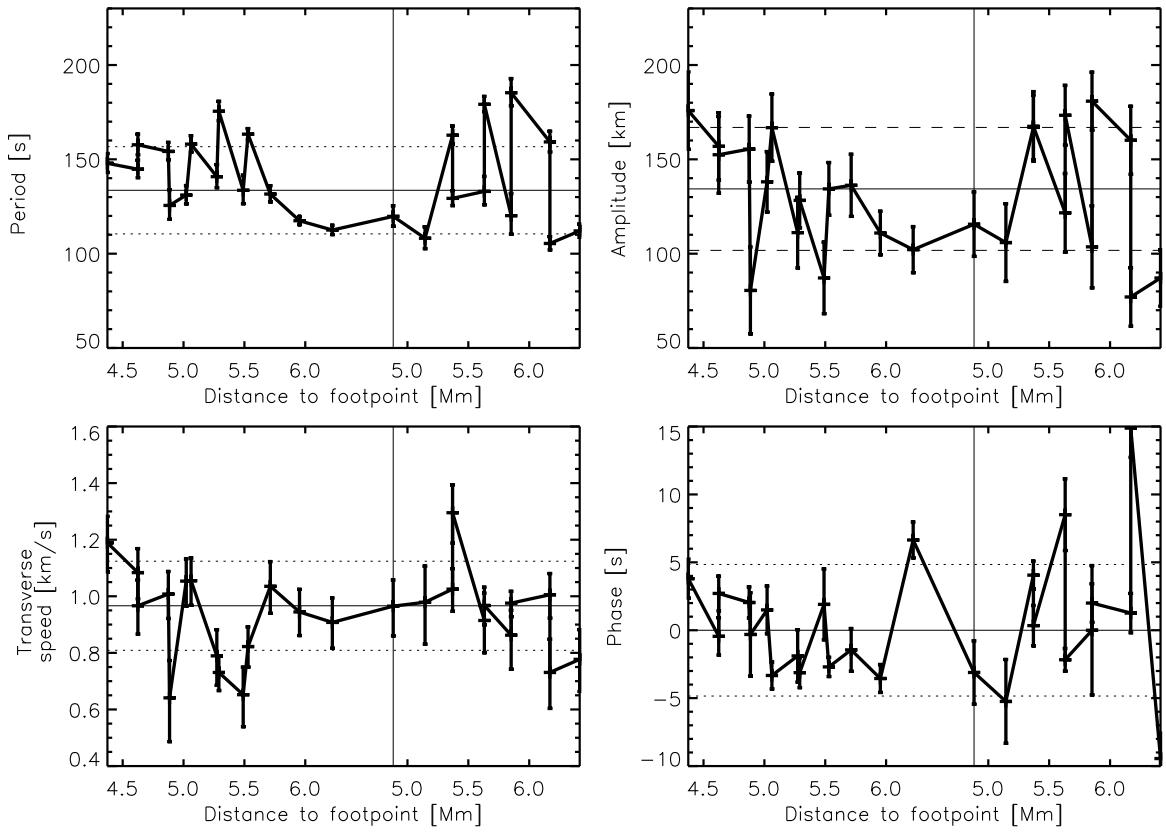

Figure 4. Fits to transverse oscillations. Top left: period. The first 15 measurements are for slit positions perpendicular to the FOI and the rest for vertical slits (see Figure 3). Error bars show the standard deviation of the fits. Top right: amplitude. Bottom left: transverse velocity, i.e., apparent motion along the slit. Bottom right: phase. Phase = 0 is the median phase of all measured oscillations.

magnetic field strength in the flux tube and the wave period:

$$B_0 = \sqrt{\frac{\mu_0}{2}}\frac{L}{P}\sqrt{\rho_0\left(1+\frac{\rho_e}{\rho_0}\right)},$$

where μ_0 is the magnetic permeability, ρ_0 and ρ_e are the internal and external densities, L is the wavelength, and P is the period.

Since it is not possible to determine a reliable phase speed from the measurements, it is difficult to compute the wavelength. We can, however, estimate a minimum value for L: the oscillations are seen in a segment approximately 1 Mm in length and the uncertainty in the phase is of the order of the cadence (3.4 s) leading to a minimum phase speed of 294 km s^{-1} and a wavelength of 40 Mm. (Note that this estimation gives no

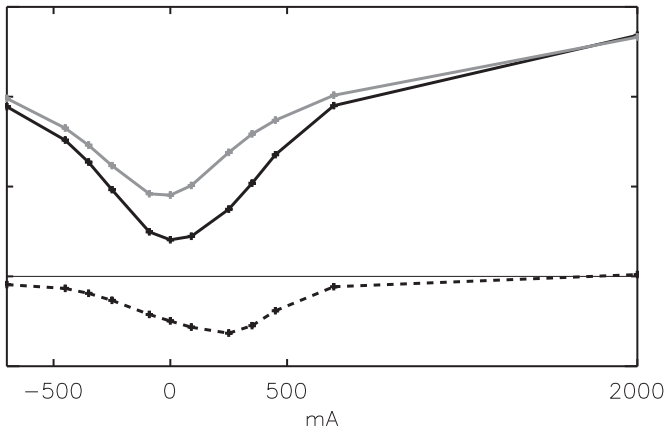

Figure 5. Average Ca II 8542 Å profile in the FOI (black solid line) and average line profile of the ROI excluding the FOI and spot (gray). The difference between the two upper profiles is indicated by the dashed black line. *Y*-axis units are arbitrary. Profiles are normalized to the local continuum.

information on the propagation direction.) This L is in agreement with estimates of wavelengths of kink waves in spicules (Kim et al. 2008). For the density we use 1.4×10^{-11} g cm^{-3}. This value was used as a density at $z = 1.25$ Mm by Judge & Carlsson (2010) to model spicules seen in Ca II H. They adopted the value based on what is a reasonable field strength in the chromosphere (well below kG) and the highly supersonic speeds observed in spicules. We will use 0.1 as the ratio of external to internal densities. (The result does not depend strongly on the ratio.) Based on these numbers and the observed periods, we estimate the fibril magnetic field strength to be 220–330 G. The mean period gives a field strength of 290 G. The corresponding Alfvén speeds are 165–250 km s^{-1}. The inferred fibril field strengths are reasonable given the location of the fibril emerging from the sunspot. Note that the wavelength, L, is the minimum wavelength based on uncertainty estimates and B_0 scales with L. If we instead use the inferred, but highly uncertain, phase speed, 190 km s^{-1} ($L = 25$ Mm), the resulting field strengths are somewhat lower, 140–210 G. (Corresponding Alfvén speeds are 100–160 km s^{-1}.) An additional large uncertainty in the field strength arises from the lack of independent density measurements in fibrils.

Note that the equation used to determine B_0 has been borrowed from coronal studies. It assumes a cylindrical geometry, zero plasma-β, and no flows. Approximating the chromospheric fibril geometry as cylindrical is reasonable, although the structures have some curvature. Van Doorsselaere et al. (2009) studied the effect of loop curvature on coronal loop kink oscillations and found that the kink wave period and damping are similar in straight cylinders with a density transition to the corona and in curved toroidal loops surrounded by a smooth transition to the corona. For a field strength of 290 G, plasma-β in the mid-chromosphere is below 0.01 (based on the Maltby et al. 1986 quiet-Sun model atmosphere). Hence the plasma-β condition is well fulfilled. Finally, the downflow speed of roughly 10 km s^{-1} is roughly an order of magnitude smaller compared to the estimated Alfvén speed, so that the results obtained from the employed equation are consistent with the conditions under which the equation is valid.

3.4. Footpoint

The FOI footpoint is at the edge of the sunspot umbra on the side with no penumbral fibrils. The Stokes I profiles are often asymmetric at the footpoint. An example profile and the time evolution of the Ca II 8542 Å line in the footpoint (i.e., where the FOI retract to) are shown in Figure 6. Some of the features in the intensity profiles may be due to the non-cotemporal wavelength sampling; there is a 20 s time delay between the most blue and most red wavelengths. The footpoint intensity time series displays a sawtooth pattern indicating steepening waves (panel (c) in Figure 6). The sawtooth pattern begins at $t = 300$–400 s also when the FOI first become clearly visible. Sawtooth patterns as strong as in the footpoint are not usually seen in the surroundings. A more diffuse sawtooth pattern is visible in the intensity time series sampling the body of the FOI. The FOI pattern may be more diffuse because the profiles originate from the fibrils as well as the atmosphere the FOI are embedded in.

The footpoint line core and continuum intensities increase once the dark fibril connects with the footpoint at $t = 1000$ s. This coincides in time with when the mostly negative Stokes V blue lobe becomes smaller in amplitude and even momentarily positive. No clear opposite polarity flux is seen in the pore or right next to it at any point in the Fe I 6302 Å data (at much lower cadence) indicating that the changes in Ca II 8542 Å may be caused by a transient heating event in the chromosphere. The footpoint intensity and Stokes V time series appear to have a 300 s periodicity, i.e., roughly twice the period of the kink wave seen in the body of the FOI.

Note that the most dynamic phase, including the apparent opposite polarity, begins at around $t = 1000$ s when the FOI come into contact with the footpoint, i.e., after the oscillations in the FOI have already begun (at $t = 800$ s); the rapid change in footpoint dynamics appears to be a consequence of the retracting fibril.

4. DISCUSSION

We have presented on-disk observations of a kink wave in an active region chromospheric fibril. The high spatial and temporal resolution of the data have allowed us to study the event in detail. It begins with a lateral movement of the fibril which has its footpoint at the edge of a sunspot umbra. The transverse oscillations of the fibril are associated with redshifted, broadened intensity profiles, while indications of steepening waves are seen in the footpoint. The period of the waves in the footpoint is roughly twice the period of the FOI transverse oscillations. The event ends as the fibril is retracted into the footpoint. It is not clear what triggers the event. One possible scenario is that the magnetic field above (at the base of the corona) changes and both the lateral movement and oscillations result from that. Since we see no strong systematic differences in measured phases in our observations, we cannot say for sure whether the disturbance propagates or, if it does, in which direction. Where a trend in measured phases is seen the propagation is downward, i.e., toward the FOI footpoint. Based on a comparison of *Hinode* observations and Monte Carlo simulations of Alfvén waves in spicules, both upward and downward propagating waves are likely (De Pontieu et al. 2007).

If the observed event is due to reconnection higher up, the observed redshift would be consistent with a bipolar jet occurring at the reconnection site (e.g., Innes et al. 1997). The largest difference between the FOI intensity profile and the average intensity profile of the surroundings is at ≈250 mÅ corresponding to a Doppler velocity of 9 km s^{-1} (Figure 5). Compared to velocities of -20 km s^{-1} seen in the Ca II 8542 Å on-disk counterparts of

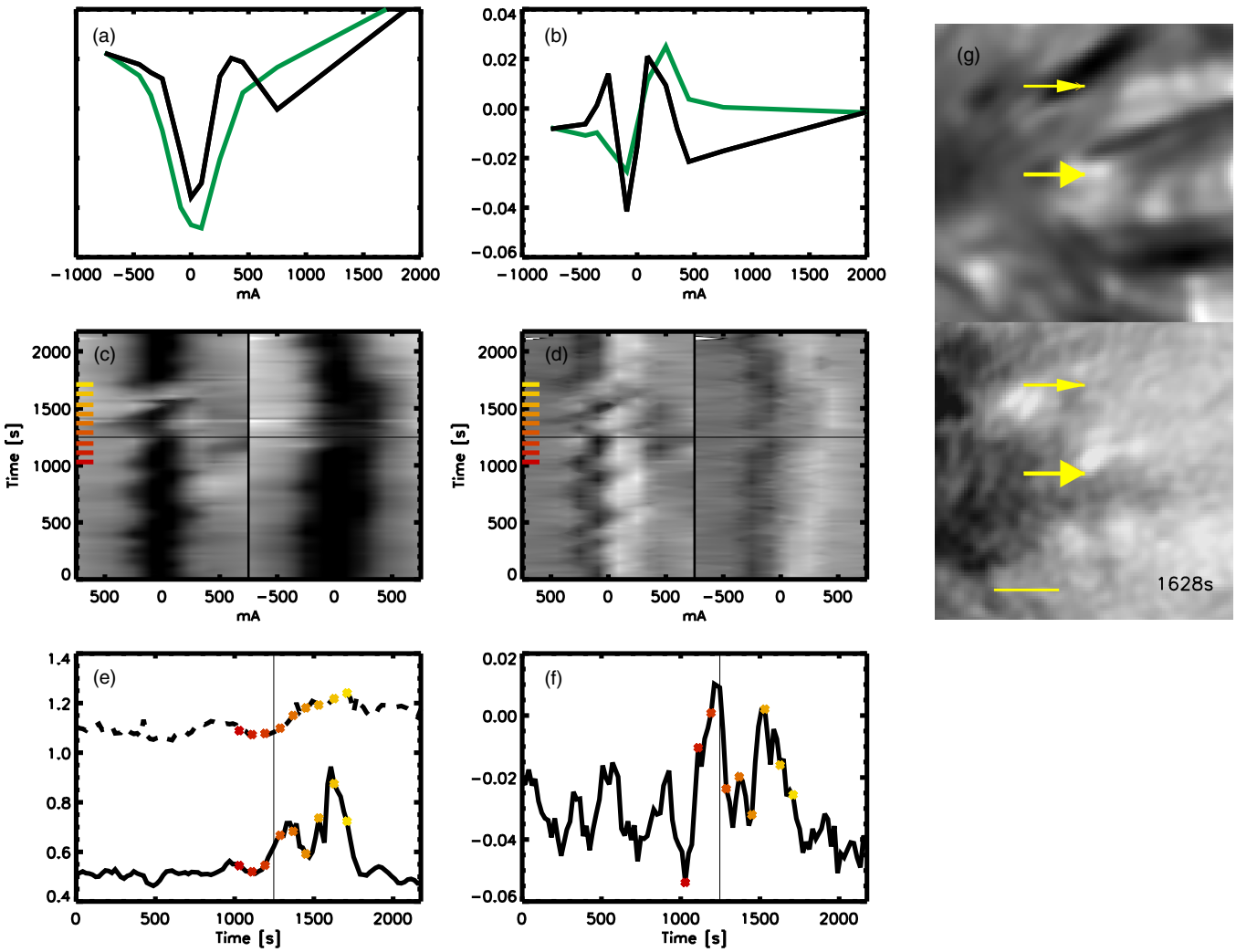

Figure 6. FOI footpoint in Ca II 8542 Å. Top panels: Stokes *I* (panel (a)) and *V* (panel (b)) profiles in the footpoint (in black) at $t = 1218$ s. The green (gray in the printed version) profiles are an average of a $2\farcs2 \times 2\farcs2$ region around the footpoint. Middle panels: time evolution of the Stokes *I* (panel (c)) and *V* (panel (d)) profiles in the footpoint (far left profile) and in a nearby pixel (far right profile). The horizontal line marks time of top panels' profiles, the colored ticks correspond to the times indicated by the asterisks in the lower panels. Bottom panels: line core (solid line) and continuum (dashed line) intensities (panel (e)) and Stokes *V* at −250 mÅ (panel (f)) in the footpoint. The vertical line shows the time of the profiles in the top panels. (g) Snapshots of Stokes *I* at 450 mÅ (top) and Stokes *V* at −250 mÅ (bottom). The large (lower) arrows mark the location of the footpoint and small (upper) arrows the pixel shown in the middle panels. The tick mark corresponds to 1 Mm.
(A color version of this figure is available in the online journal.)

type II spicules (rapid blueshifted events; Rouppe van der Voort et al. 2009), the FOI velocity does not seem very high. Shoji & Kurokawa (1995) observed downflows of up to 50–100 km s^{-1} in Hα and Ca K during the impulsive phases of two flares. They also observed Na I D1 and D2 lines as well as metallic lines which showed significantly smaller, up to 2–6 km s^{-1}, downflows. Based on the above, the magnitude of the FOI redshift does not exclude a small-scale reconnection event higher up in the atmosphere as the trigger of the observed dynamics (no flares were recorded during the observation day, so it can only be a small event). A scenario involving a small-scale reconnection event is also supported by the apparent change in the Ca II 8542 Å Stokes *V* polarity in the footpoint and the increased line and continuum intensities when the FOI connect to the footpoint. These can be interpreted as an emission feature near the line core caused by transient heating in the chromosphere (Sánchez Almeida 1997).

Fast and slow MHD waves may be coupled due to effects of boundary conditions, inhomogeneities, and gas pressure. Coupling of MHD waves is a possible explanation for the combined EIT and *Transition Region and Coronal Explorer* (*TRACE*) observations of loop footpoint intensity variations having the same period as the co-occurring fast transverse loop oscillation (Verwichte et al. 2010). This was demonstrated by Terradas et al. (2011), who show how transverse motions of a coronal loop can produce slow waves with the same periodicity as the transverse oscillation. A coupling of MHD waves may be the connection between the observed FOI oscillations and the steepening waves. Note that unlike in the coronal loop case, the observed steepening (indicating the presence of shocks) wave has a period roughly twice that of the FOI oscillation.

The mean period, amplitude, and phase speed of the oscillations are similar to measurements in off-limb spicules (e.g., He et al. 2009 at heights below 2 Mm). The properties of the oscillations allowed us to estimate the field strength in the dynamic fibril to be at least 220–330 G. For comparison, a value of 120 G at the base of the corona was used by De Pontieu et al. (2004) to model spicules via leakage of P-modes into the chromosphere. Centeno et al. (2010) estimate, based on He I 10830 Å triplet Hanle and Zeeman measurements, 50 G as a possible lower

value for the field in network spicules. López Ariste & Casini (2005) measured 30 G fields at a height of 3000–5000 km above the limb. Considering that we observed an active region and the magnetic field strength decreases with height (the Ca II 8542 Å on-disk observations are at heights below 1500 km) a field strength of a few hundred gauss is reasonable. It is also consistent with the chromospheric field strength near the outer boundary of a sunspot (e.g., Solanki et al. 2003; Orozco Suarez et al. 2005). Once a telescope model for the Ca II 8542 Å line becomes available, it will be interesting to compare this value with results from Zeeman measurements.

How common kink waves in fibrils are is difficult to estimate, though the similarity with kink waves in spicules suggests that the two should have similar occurrence rates. We see indications of a few more such oscillations in the data, but they are not as clear as the one presented here. For the oscillation to be visible the spatial and temporal resolutions need to be high. Also, the choice of wavelength may play a role: perhaps the oscillations were so clearly visible because the fibril was strongly redshifted with respect to the surroundings. Due to the complex optically thick background consisting of other fibrils, the visibility of the oscillations on the disk is limited compared to the optically thin limb spicules.

5. SUMMARY

We identified kink waves in an active region fibril in high spatial and temporal resolution Ca II 8542 Å data. The characteristics agree with observations of kink waves in off-limb spicules. The properties, e.g., periods and velocity amplitudes, measured by He et al. (2009) for kink waves seen in *Hinode* Solar Optical Telescope Ca H imaging data at heights below 2 Mm (relative to the reconnection site) are similar to those found in our on-disk observations. The momentarily reverse polarity in Ca II 8542 Å Stokes *V* profiles together with increased intensity points to a small-scale reconnection event higher in the atmosphere as the trigger. To our knowledge this is the first observation of chromospheric kink waves on the solar disk. Based on the measured wave phase and period we estimate the dynamic fibril field strength to be a few hundred gauss.

This work was partly supported by WCU grant No. R31-10016 from the Korean Ministry of Education, Science and Technology. The Swedish Solar Telescope (SST) is operated on the island of La Palma by the Institute for Solar Physics of the Royal Swedish Academy of Sciences in the Spanish Observatorio del Roque de los Muchachos of the Instituto de Astrofísica de Canarias. We thank the telescope staff for their kind support with the SST.

REFERENCES

Axford, W. I., & McKenzie, J. F. 1992, in Solar Wind Seven Colloquium, ed. E. Marsch & R. Schwenn (Oxford: Pergamon), 1
Centeno, R., Trujillo Bueno, J., & Asensio Ramos, A. 2010, ApJ, 708, 1579
Choudhuri, A. R., Auffret, H., & Priest, E. R. 1993, Sol. Phys., 143, 49
De Pontieu, B., Erdélyi, R., & James, S. P. 2004, Nature, 430, 536
De Pontieu, B., McIntosh, S. W., Carlsson, M., et al. 2007, Science, 318, 1574
De Pontieu, B., McIntosh, S. W., Carlsson, M., et al. 2011, Science, 331, 55
Erdélyi, R., & Fedun, V. 2007, Science, 318, 1572
He, J., Marsch, E., Tu, C., & Tian, H. 2009, ApJ, 705, L217
Hollweg, J. V. 1981, Sol. Phys., 70, 25
Huang, P., Musielak, Z. E., & Ulmschneider, P. 1995, A&A, 297, 579
Innes, D. E., Inhester, B., Axford, W. I., & Wilhelm, K. 1997, Nature, 386, 811
Judge, P. G., & Carlsson, M. 2010, ApJ, 719, 469
Kim, Y., Bong, S., Park, Y., et al. 2008, J. Korean Astron. Soc., 41, 173
Kukhianidze, V., Zaqarashvili, T. V., & Khutsishvili, E. 2006, A&A, 449, L35
López Ariste, A., & Casini, R. 2005, A&A, 436, 325
Maltby, P., Avrett, E. H., Carlsson, M., et al. 1986, ApJ, 306, 284
Musielak, Z. E., & Ulmschneider, P. 2001, A&A, 370, 541
Nakariakov, V. M., & Ofman, L. 2001, A&A, 372, L53
Nakariakov, V. M., & Verwichte, E. 2005, Living Rev. Sol. Phys., 2, 3
Orozco Suarez, D., Lagg, A., & Solanki, S. K. 2005, in Proc. Int. Scientific Conf. on Chromospheric and Coronal Magnetic Fields, ed. D. E. Innes, A. Lagg, & S. A. Solanki (ESA SP-596; Noordwijk: ESA), 59
Pasachoff, J. M., Noyes, R. W., & Beckers, J. M. 1968, Sol. Phys., 5, 131
Roberts, B. 1979, Sol. Phys., 61, 23
Rouppe van der Voort, L., Leenaarts, J., de Pontieu, B., Carlsson, M., & Vissers, G. 2009, ApJ, 705, 272
Sánchez Almeida, J. 1997, A&A, 324, 763
Scharmer, G. B. 2006, A&A, 447, 1111
Scharmer, G. B., Dettori, P. M., Lofdahl, M. G., & Shand, M. 2003, Proc. SPIE, 4853, 370
Selbing, J. 2005, PhD thesis, Stockholm Observatory
Shoji, M., & Kurokawa, H. 1995, PASJ, 47, 239
Singh, K. A. P., & Dwivedi, B. N. 2007, New Astron., 12, 479
Solanki, S. K., Lagg, A., Woch, J., Krupp, N., & Collados, M. 2003, Nature, 425, 692
Spruit, H. C. 1981, A&A, 98, 155
Terradas, J., Andries, J., & Verwichte, E. 2011, A&A, 527, A132
Trujillo Bueno, J., Merenda, L., Centeno, R., Collados, M., & Landi Degl'Innocenti, E. 2005, ApJ, 619, L191
Tsiropoula, G., Alissandrakis, C. E., & Schmieder, B. 1994, A&A, 290, 285
Van Doorsselaere, T., Nakariakov, V. M., & Verwichte, E. 2008, ApJ, 676, L73
van Doorsselaere, T., Verwichte, E., & Terradas, J. 2009, Space Sci. Rev., 149, 299
van Noort, M., Rouppe van der Voort, L., & Löfdahl, M. G. 2005, Sol. Phys., 228, 191
Verwichte, E., Foullon, C., & Van Doorsselaere, T. 2010, ApJ, 717, 458
Yi, Z., Darvann, T. A., & Molowny Horas, R. L. 1992, LEST Found., Tech. Rep., 56
Zaqarashvili, T. V., & Erdélyi, R. 2009, Space Sci. Rev., 149, 355
Zaqarashvili, T. V., Khutsishvili, E., Kukhianidze, V., & Ramishvili, G. 2007, A&A, 474, 627